catalysts

MDPI

Article

An Insight into Synergistic Metal-Oxide Interaction in CO_2 Hydrogenation to Methanol over Cu/ZnO/ZrO_2

Xiao Chang [1,†], Xiaohui Zi [1,†], Jing Li [2], Fengdong Liu [2], Xiaoyu Han [3], Jiyi Chen [3], Ziwen Hao [3], Heng Zhang [1], Zhenmei Zhang [3], Pengju Gao [1], Maoshuai Li [1,*], Jing Lv [1] and Xinbin Ma [1]

[1] Key Laboratory for Green Chemical Technology of Ministry of Education, Collaborative Innovation Center of Chemical Science and Engineering, National Industry-Education Integration Platform of Energy Storage, School of Chemical Engineering and Technology, Tianjin University, Tianjin 300350, China; changx_97@tju.edu.cn (X.C.); zxh440@tju.edu.cn (X.Z.); hgxy_zhangheng@tju.edu.cn (H.Z.); gaopen_gju@tju.edu.cn (P.G.); muddylj@tju.edu.cn (J.L.); xbma@tju.edu.cn (X.M.)

[2] State Key Laboratory of Solid Waste Reuse for Building Materials, Beijing Building Materials Academy of Science Research, Beijing 100041, China; lj02041988@163.com (J.L.); liufengdong@bbma.com.cn (F.L.)

[3] Joint School of National University of Singapore and Tianjin University, International Campus of Tianjin University, Binhai New City, Fuzhou 350207, China; xiaoyuhan@u.nus.edu (X.H.); jiyichen@u.nus.edu (J.C.); ziwenhao@u.nus.edu (Z.H.); zhenmei_zhang@u.nus.edu (Z.Z.)

* Correspondence: maoshuaili@tju.edu.cn

† The authors contribute equally to this study.

Abstract: The metal-oxide interaction is of significance to the construction of active sites for Cu-catalyzed CO_2 hydrogenation to methanol. This study examines the effect of ZnO and ZrO_2 composition on the Cu/ZnO/ZrO_2 catalyst structure and surface properties to further tune the catalytic activity for methanol synthesis. The ZnO/ZrO_2 ratio can impact the CuZn alloy formation from strong Cu-ZnO interactions and the surface basic sites for CO_2 adsorption at the Cu-ZrO_2 interface. The proportional correlation of the CuZn alloy content and CO_2 desorption amount with the space-time yield (STY) of methanol reveals a synergistic interaction between Cu and oxides (ZnO and ZrO_2) that enhances methanol synthesis. The optimized Cu/ZnO/ZrO_2 catalyst exhibits higher STY relative to the traditional Cu/ZnO/Al_2O_3 catalyst. The obtained results presented herein can provide insight into the catalyst design for methanol synthesis from CO_2.

Keywords: CO_2 hydrogenation; methanol; Cu-based catalyst; Cu-ZrO_2 interaction; CuZn alloy

Citation: Chang, X.; Zi, X.; Li, J.; Liu, F.; Han, X.; Chen, J.; Hao, Z.; Zhang, H.; Zhang, Z.; Gao, P.; et al. An Insight into Synergistic Metal-Oxide Interaction in CO_2 Hydrogenation to Methanol over Cu/ZnO/ZrO_2. *Catalysts* **2023**, *13*, 1337. https://doi.org/10.3390/catal13101337

Academic Editors: Zhong-Wen Liu and Giuseppe Bonura

Received: 13 September 2023
Revised: 28 September 2023
Accepted: 29 September 2023
Published: 30 September 2023

1. Introduction

The production process of methanol, a high-value-added chemical, has historically received widespread attention. As early as 1923, BASF Company in Germany took the lead in developing high-pressure methanol synthesis technology from syngas [1]. Afterward, ICI discovered a low-pressure process for the synthesis of CH_3OH using Cu-based catalysts [2]. Recently, Bai et al. [3] proposed that CO_2 from the atmosphere and H_2 from renewable energy sources can be used for CO_2 hydrogenation to methanol, which can realize chemical utilization of CO_2 and storage of renewable energy.

CO_2 hydrogenation to methanol is an exothermic reaction, with high-pressure and low-temperature conditions being thermodynamically beneficial for it. However, CO_2 molecules are relatively stable, which makes CO_2-to-methanol conversion difficult at low temperatures. At higher temperatures, CO_2 is prone to reverse water-gas shift (RWGS), which is an endothermic reaction that generates by-product CO and reduces the methanol selectivity.

$$CO_2 + 3H_2 \rightarrow CH_3OH + H_2O,\ \Delta H_{298K} = -49.5\ kJ/mol \quad (1)$$

$$CO_2 + H_2 \rightarrow CO + H_2O,\ \Delta H_{298K} = 41.2\ kJ/mol \quad (2)$$

CO_2 hydrogenation to methanol catalysts can be roughly divided into Cu-based [4–14], precious metal (Au [15,16], Ag [17], Pt [18], etc.), bimetallic (Cu-Pd [19], Zn-Pd [20], Co-Pd [21], etc.), and oxide (In_2O_3) catalysts [22–25]. The $Cu/ZnO/Al_2O_3$ catalyst developed by ICI can also be applied to the CO_2 hydrogenation to methanol. However, the catalytic performance bears room for improvement, and the presence of water in the product can promote the sintering of Cu and ZnO, leading to catalyst deactivation [26]. It is of importance to develop highly active and stable Cu-based catalysts for methanol synthesis from CO_2.

The existing literature endeavors to design efficient active sites for Cu-based catalysts. However, there is no consensus on the active site structure due to the catalyst complexity. A synergistic effect between Cu and oxide (e.g., ZnO, ZrO_2, and CeO_2) at the interface has been proposed as the active site [7]. Another view is that CuZn alloy is an active site; its formation may promote the partial reduction of ZnO to Zn^{q+} or Zn^0, thereby modifying the Cu surface [9,11,27]. The dissociated H atom on Cu^0 might overflow to the CuZn alloy, and then react with the adsorbed species CO_2* by ZnO near the CuZn alloy, so as to improve the catalyst performance in the CO_2 hydrogenation to methanol [28]. Compared to syngas, CO_2 hydrogenation to methanol produces water, which requires a weakly hydrophilic material to timely desorb the generated water. In previous work [29], a highly dispersed $Cu-ZrO_2$ interface can effectively improve the conversion rate and methanol selectivity. Meanwhile, compared to Al_2O_3, ZrO_2 shows weaker hydrophilicity. In this work, we propose the design of a tertiary $Cu\text{-}ZnO-ZrO_2$ catalyst with the construction of Cu-ZnO and $Cu-ZrO_2$ interactions as active centers, which potentially promotes CO_2 hydrogenation to methanol.

In this study, Cu/ZnO, Cu/ZrO_2, and $Cu/ZnO/ZrO_2$ with a series of mass ratios of ZnO/ZrO_2 were constructed with the structure and surface properties studied using a range of characterizations [e.g., XRD (powder X-ray diffraction), TEM (transmission electron microscopy), XPS (X-ray photoelectron spectra), and CO_2-TPD (CO_2 temperature-programmed desorption)]. The optimized $Cu/ZnO/ZrO_2$ catalyst outperforms the conventional $Cu/ZnO/Al_2O_3$ catalyst in terms of activity for CO_2 hydrogenation to methanol. The presence of CuZn alloy and $Cu-ZrO_2$ interaction enhances CO_2 conversion and methanol formation rates.

2. Results and Discussion

2.1. Characterization

A series of $Cu/ZnO/ZrO_2$ catalysts with different ZnO/ZrO_2 mass ratios were synthesized via oxalate coprecipitation. The catalysts were named based on element content. For example, the ZnO/ZrO_2 ratio is 2:5 in the catalyst, which is named C3Z2Z5. The element contents measured using ICP-OES (inductively coupled plasma optical emission spectroscopy) are close to the target values [Table 1, including specific surface area (S_{BET}), specific surface area of Cu (S_{Cu}), Cu dispersion (D_{Cu}), Cu diameters (d_{Cu}), and other physicochemical properties] indicative of no significant loss of Cu during the catalyst preparation. In the adsorption and desorption isotherms (Figure S1A), all the catalysts show typical Type IV hysteresis loops, indicating that the prepared catalysts are mesoporous. The pore size distribution in Figure S1B also confirms the mesoporous structure. As the ZnO/ZrO_2 ratio increases, the specific surface area shows a decreasing trend, which is not conducive to the dispersion of Cu (Table 1). This indicates that ZrO_2 plays an important role in maintaining the specific surface area of the $Cu/ZnO/ZrO_2$ catalyst. In the Zr-containing catalysts, the change in ZnO/ZrO_2 ratio does not have a significant impact on the pore volume. Compared with Cu/ZrO_2 and $Cu/ZnO/ZrO_2$, the pore volume of Cu/ZnO is significantly reduced. The pore size shows an increasing trend with the increase of the ZnO/ZrO_2 ratio.

Table 1. Physicochemical properties of the catalysts.

Samples	Cu (wt%) [a]	S_{BET} (m^2/g)	Pore Volume (cm^3/g)	Pore Size (mm)	D_{Cu} (%) [b]	d_{Cu} (nm) [b]	S_{Cu} (m^2/g_{cat}) [b]	S_{Cu} (m^2/g_{Cu}) [b]	H_2 Uptake (mmol/g_{cat})	CO_2 Desorption (mmol/g_{cat})
C3Z0Z7	28.62	95.5	0.41	13.0	7.11	14.6	13.10	45.79	0.0147	0.244
C3Z1Z6	28.89	94.4	0.40	13.1	4.74	21.9	8.82	30.52	0.0147	0.278
C3Z2Z5	30.80	88.7	0.44	15.2	4.12	25.2	8.18	26.57	0.0148	0.311
C3Z3Z4	30.73	80.5	0.45	17.1	3.60	28.9	7.13	23.21	0.0139	0.250
C3Z4Z3	28.54	71.5	0.51	21.9	2.73	38.0	5.02	17.62	0.0141	0.203
C3Z5Z2	28.19	71.0	0.49	20.0	3.12	33.3	5.67	20.12	0.0155	0.180
C3Z6Z1	30.22	70.7	0.50	21.0	2.72	38.3	5.29	17.52	0.0161	0.117
C3Z7Z0	31.13	30.7	0.27	28.6	—	—	0.97	3.13	0.0092	0.061

[a] Derived from ICP-OES. [b] Derived from N_2O titration.

The crystalline structures of all the catalysts after calcination and reduction were analyzed by XRD (Figure 1). The monoclinic CuO (2θ = 35.5° and 38.7°, PDF#48-1548) was observed in all the calcined samples in Figure 1A, while ZnO (2θ = 31.8°, 34.4° and 38.7°, PDF#79-0206) [30,31] can only be detected when the Zn content exceeds 20 wt%. The ZrO_2 in all samples was a-ZrO_2, because of the low calcination temperature, and no characteristic peak of ZrO_2 was observed. The monoclinic CuO phase was reduced to a cubic metallic Cu^0 phase (2θ = 43.3°, 50.4°, and 74.1°, PDF#4-836) and Cu_2O (2θ = 37.1°, PDF#65-3288) via H_2 reduction at 300 °C in Figure 1B [32,33]. As the ZnO/ZrO_2 ratio increased, the Cu reflection signal intensified, indicating that metal Cu continued to aggregate. In Figure 1C, it is worth noting that the Cu characteristic diffraction peak (2θ = 43.3°) moved to lower degrees as the ZnO content increased. This indicates that during the catalyst reduction activation process, a fraction of ZnO is reduced to Zn^0 and interacts with Cu to form a CuZn alloy [34,35].

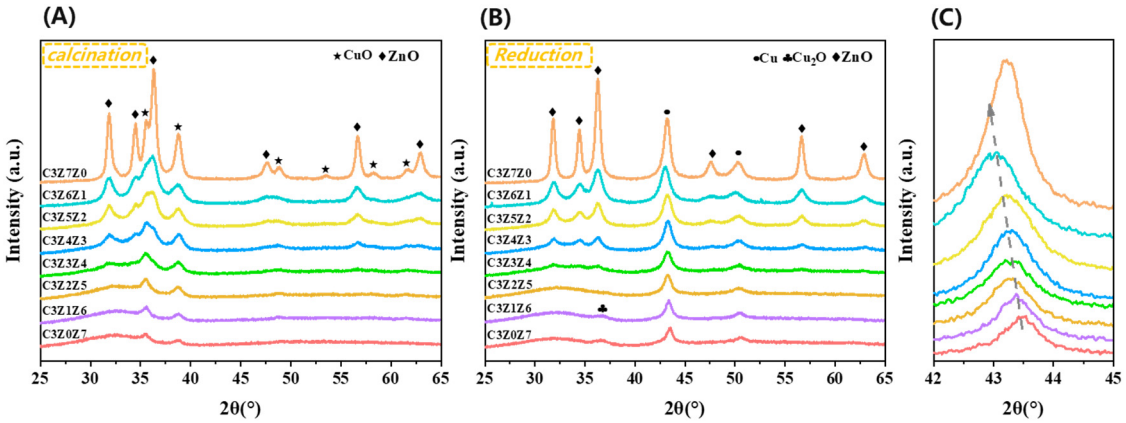

Figure 1. XRD patterns of calcined (**A**) and reduced (**B**,**C**) catalysts.

The TEM image (Figure S2) shows that the reduced catalyst exhibits irregular morphology, with a size ranging approximately from 400–600 nm. In Cu/ZrO_2 and Cu/ZnO/ZrO_2, the black area weakly increased with the ZnO content increased, due to Cu aggregation. However, when the ZrO_2 content decreased from 10% (C3Z6Z1) to 0% (C3Z7Z0), the size of Cu particles increased significantly, which is consistent with the XRD analysis. The size of Cu particles in Cu/ZnO is significantly larger than that in Cu/ZrO_2, which suggests that ZrO_2 has a stronger dispersion effect on Cu than ZnO [36]. Regular hemispherical or spherical Cu nanoparticles can be found in the HR-TEM images (Figure 2). In the C3Z1Z6 sample, Cu particles expose the (100) and (111) crystal planes corresponding to the lattice spacing = 0.182 and 0.210 nm, and ZnO particles expose the (101) crystal planes corresponding to the lattice spacing = 0.248 nm [37]. As the ZnO/ZrO_2 mass ratio increased, Cu (111) crystal plane lattice spacing expanded to 0.216–0.219 nm. The expansion of lattice stripes indicates that during the reduction process, ZnO is reduced to Zn^0 and combines with the metallic Cu to form a CuZn alloy, which is consistent with the XRD result [35,38]. No lattice

fringe of ZrO_2 was found in the HR-TEM image, which is related to the amorphous morphology of ZrO_2. EDS-mapping (Energy Dispersive Spectrometer mapping) was used to determine the distribution of Cu, Zn, and Zr in the catalyst. In Figure S3, as the ZnO/ZrO_2 ratio increased, the metallic Cu^0 particles were gradually aggregated.

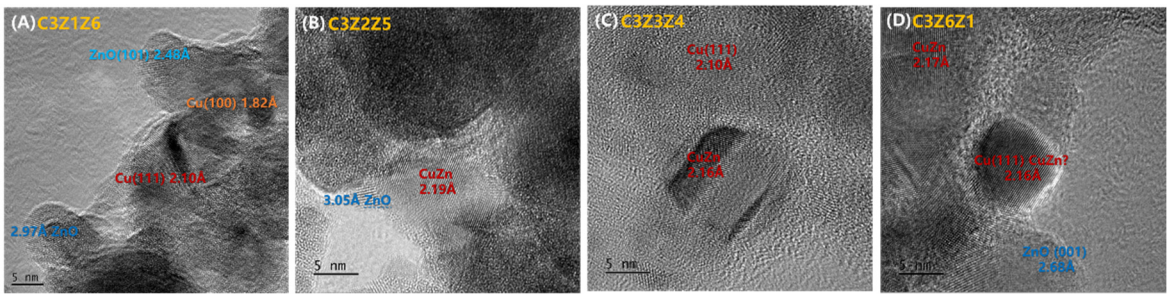

Figure 2. HR-TEM images of reduced catalysts.

N_2O-oxidation followed by H_2 titration was used to calculate the S_{Cu}, D_{Cu}, and d_{Cu} (Table 1). As the ZnO/ZrO_2 ratio increases, metallic Cu^0 particles gradually aggregate, reasonably agreeing with the TEM and XRD analyses. Due to the presence of CuZn alloy in the sample, the Cu particle size calculated from the N_2O titration is too large, so the results are considered principally for qualitative analysis.

The H_2-TPR (H_2-temperature-programmed reduction) analysis (Figure 3) for the calcined catalysts generated overlapped hydrogen consumption peaks with resultant asymmetric profiles in the 100–230 °C temperature range. In the catalysts with the ZnO/ZrO_2 ratio between 0:7 and 5:2, the three peaks (denoted as α, β, and γ) suggest the presence of different CuO species. Within this range, as the ZnO/ZrO_2 ratio increased, α peak intensity gradually decreased, indicating a decrease in content of smaller Cu particles. At the same time, β and γ peaks gradually became dominant. The reduction temperature first decreases and then increases as the ZnO/ZrO_2 ratio increases, and the C3Z2Z5 catalyst shows the lowest reduction temperature. This indicates that when the ZnO/ZrO_2 ratio is 2:5, the interaction between Cu and oxide support is strong, promoting the reduction of Cu species [39]. Only β and γ peaks were found in the C3Z6Z1 and C3Z7Z0 catalyst, which demonstrate the Cu species in the sample are mostly large CuO particles or exist in the form of bulk CuO. The theoretical H_2 reduction consumption was calculated and compared with the actual H_2 reduction consumption (Table 2). The ratio was recorded as $R_{H2/Cu}$, with $R_{H2/Cu} > 1$, indicating that ZnO was partially reduced to Zn^0.

The chemical states of Cu, Zn, and Zr on the catalyst surface can be analyzed by XPS (Figure 4). In the Cu 2p XPS spectra of the reduced catalyst (Figure 4A), the signals at binding energy (BE) = 932.6 eV and 952.4 eV belong to the characteristic peaks of Cu $2p_{3/2}$ and Cu $2p_{1/2}$. No Cu^{2+} satellite peak near 943.0 eV was observed, indicating that the surface CuO species were completely reduced [40,41]. The Cu LMM Auger region was used to better distinguish between Cu^0 and Cu^+. However, there is a certain overlap in the characteristic peak positions of Cu and Zn, so only samples with a ZnO/ZrO_2 ratio less than 2:5 were analyzed by Cu LMM. In Figure 4C, the characteristic peaks of Cu^0 or Cu^+ appeared at binding energies of 569.9 eV and 573.9 eV, but the content of Cu^+ was relatively low. After reduction, most of the Cu on the catalyst surface existed in the form of Cu^0.

The characteristic peaks of Zr $3d_{5/2}$ and Zr $3d_{3/2}$ at BE = 181.8 eV and 184.2 eV were observed in the reduced catalysts (Figure 4B). At the same time, the reduction of the catalysts did not cause a significant shift in the position of the Zr 3d characteristic peak, indicating that the surface ZrO_2 was basically not reduced to metal Zr. It can be inferred that the excessive consumption of H_2 in H_2-TPR is mainly related to the reduction of ZnO. The valence state distribution of Zn in the catalysts after reduction was analyzed by Zn LMM (Figure 4D). In C3Z2Z5, C3Z5Z2, and C3Z7Z0 catalysts, the characteristic peaks of Zn appeared at Kinetic energy = 988.0 eV, 991.2 eV, and 992.4 eV, respectively, corresponding

to Zn^{2+}, Zn^{q+}, and Zn^0. The presence of Zn^0 further clarifies that some ZnO was reduced to metal Zn during the reduction process. As the ZnO/ZrO_2 ratio increases, the content of Zn^0 shows a trend of first increasing and then decreasing.

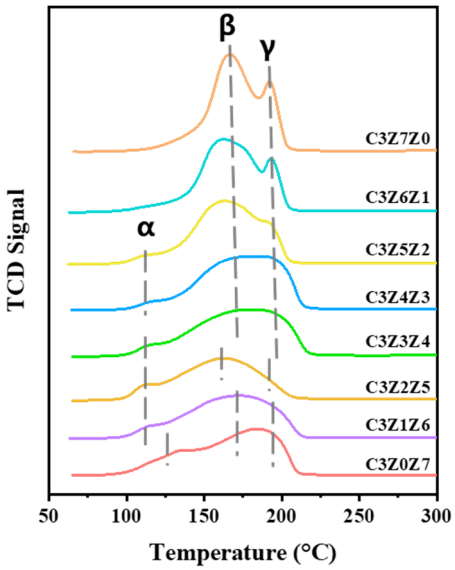

Figure 3. H_2-TPR profiles for all the catalysts.

Table 2. H_2 consumption during the TPR analysis.

Samples	Temperature °C	Actual H_2 Reduction Consumption mmol/g	Theoretical H_2 Reduction Consumption mmol/g	$R_{H2/Cu}$
C3Z0Z7	184.6	4.48	4.20	1.07
C3Z1Z6	172.9	4.49	4.24	1.06
C3Z2Z5	162.4	4.86	4.50	1.08
C3Z3Z4	179.9	4.99	4.48	1.11
C3Z4Z3	182.1	5.35	4.18	1.28
C3Z5Z2	163.2	5.34	4.14	1.29
C3Z6Z1	163.1	5.50	4.42	1.25
C3Z7Z0	164.6	5.89	4.54	1.30

In the process of CO_2 hydrogenation to methanol, the capacity of the catalyst adsorption/activation of CO_2 and H_2 plays an important role. In Cu/ZrO_2 and $Cu/ZnO/ZrO_2$, the difference in H_2 adsorption capacity (based on per gram catalyst, Table 1) is not significant, which means that the ZnO/ZrO_2 ratio has a small impact on H_2 adsorption. In the Cu/ZnO catalyst (C3Z7Z0), the adsorption capacity of H_2 is significantly lower, which is related to the larger size of Cu particles on ZnO. The larger Cu particle size reduces the adsorption sites of H_2, causing a decrease in the adsorption capacity of H_2. In the H_2-TPD (H_2 chemisorption) profile (Figure 5A) for the catalysts containing Zr, a main desorption peak of 380–420 °C can be observed, which is the desorption peak of H species bound by Cu-H bonds on metal Cu [42]. As the ZnO/ZrO_2 ratio increases, the peak temperature firstly shifts towards low temperature and then remains basically unchanged, indicating that the formation of CuZn alloy will reduce the desorption temperature of H_2. In Cu/ZnO (C3Z7Z0), the desorption temperature further decreases. In the range of the ZnO/ZrO_2 ratio between 1:6 and 5:2, the high temperature peak of 500–600 °C in H_2-TPD did not appear in the H_2-MS spectra (Figure 5B), which may be related to the unknown species released from the catalyst decomposition under high-temperature conditions (higher than the catalyst calcination temperature).

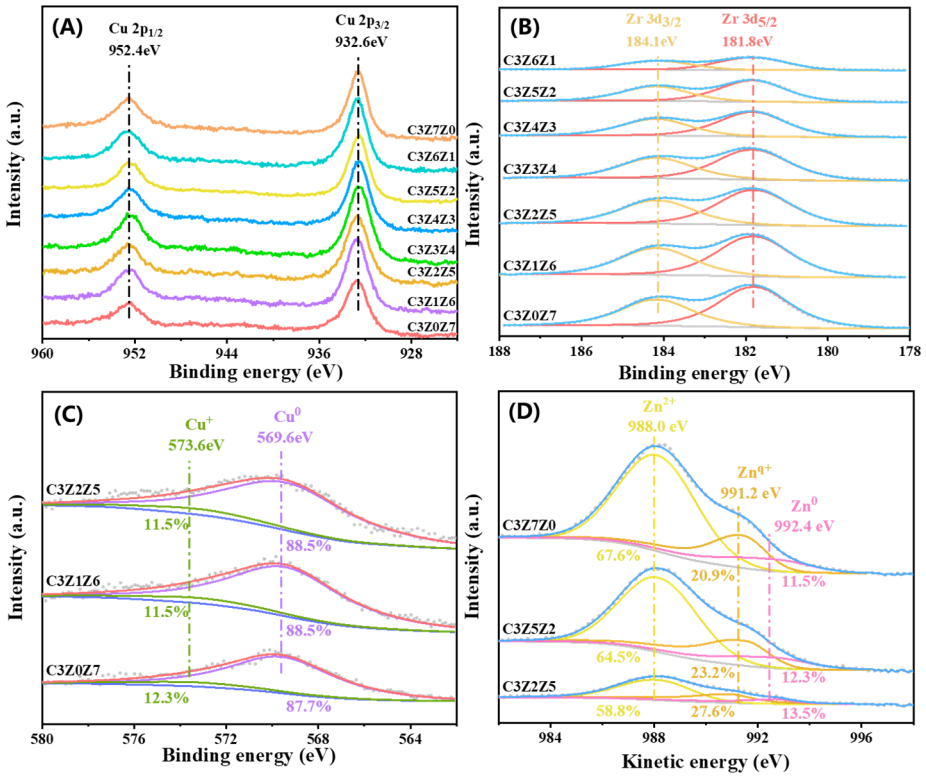

Figure 4. (**A**) Cu 2p XPS, (**B**) Zr 3d XPS, (**C**) Cu LMM, and (**D**) Zn LMM Auger spectra of reduced catalysts.

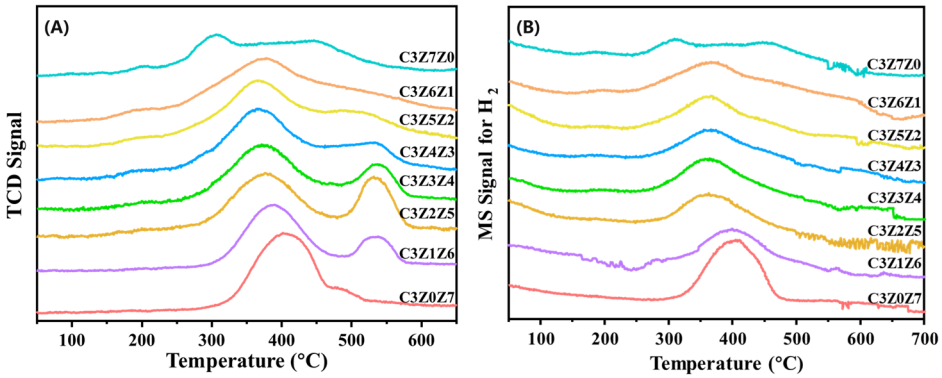

Figure 5. (**A**) The H_2-TPD, (**B**) MS-H_2 profiles.

A total of three main desorption signals were detected in the CO_2-TPD analysis (Figure 6A), including the low-temperature (80–150 °C), medium-temperature (350–450 °C), and high-temperature (450–620 °C) ranges. The difference in ZnO/ZrO_2 ratio affects the CO_2 desorption amount and temperature within different temperature ranges. With the increase of the ZnO/ZrO_2 ratio, the desorption amount in the low-temperature range decreases to a certain extent, but the desorption temperature does not significantly increase. In the middle-temperature range, the CO_2 desorption amount is relatively low in each catalyst and the change is not significant, but the desorption temperature gradually increases. The CO_2 desorption amount in the high-temperature zone reaches a maximum value on C3Z2Z5 and then decreases. The desorption temperature is basically the same in the samples containing Zn but is higher than that in C3Z0Z7. The CO_2 desorption amount (Table 1) depends on the ZnO and ZrO_2 composition. The value firstly increases and then decreases with increasing ZnO/ZrO_2 ratio and the highest amount (0.311 mmol/g_{cat}) is recorded at the ratio of 2:5.

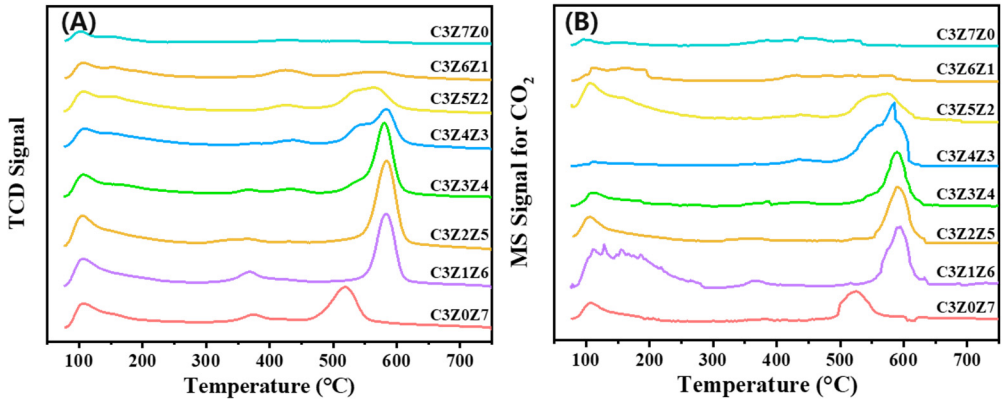

Figure 6. (**A**) The CO_2-TPD, (**B**) MS-CO_2 profiles.

The CO_2 desorption peaks correspond to three basic sites on the catalyst surface, namely weak, moderate, and strong basic sites. At weak basic sites, CO_2 adsorbs as bicarbonate and desorbs at low temperatures [6,39]. The moderate basic sites are generally metal-O pairs, which adsorb CO_2 and form carbonate species [43]. At medium temperature, the carbonate intermediate is prone to RWGS, generating CO [44]. The species generated by CO_2 adsorption on strongly basic sites are not yet clear, but it can be determined that the presence of strongly basic sites is related to the Cu-ZrO_2 interface [29,45–47]. CO_2 hydrogenation to methanol is generally operated at 200–300 °C. Therefore, the moderate and strong basic sites are effective active sites for CO_2 adsorption/activation and further conversion. The difference in ZnO/ZrO_2 ratio affects the types and quantities of basic sites on the carrier surface and changes the desorption amount and temperature of CO_2.

2.2. Catalytic Test

Catalytic performance comparison of CuZn (C3Z7Z0), CuZr (C3Z0Z7), CuZnZr (C3Z2Z5), and commercial catalyst (CuZnAl) for the reaction is shown in Figure 7A. The CO_2 conversion increases with the increasing temperature. The order of CO_2 conversion follows CuZnAl > CuZnZr > CuZr > CuZn. Methanol selectivity is decreased with increasing temperature (Figure 7B). Except for CuZnAl, the methanol selectivity remains above 60% at 240 °C, indicating that the higher CO_2 conversion over CuZnAl is due to the generation of more by-product CO. The methanol selectivity for the catalysts follows the order CuZr > CuZn ≈ CuZnZr > CuZnAl. STY of methanol was used to determine catalyst activity for methanol synthesis (Figure 7C). The STY of methanol rises with the increase in temperature (180–260 °C). CuZnZr shows the best catalytic performance in all four catalysts, which also ranks top in the existing literature (Table S1). In traditional CO_2 hydrogenation to methanol catalysts, CuZn alloy [9,27,28] or Cu-ZnO interface [48] is generally considered as the active site. Here we can note that the CuZn sample displays the lowest Cu surface area with the smallest amount for reactant uptake, which can be considered to be responsible for the poor activity for methanol formation. Meanwhile, CuZr shows the highest dispersion and largest surface area of Cu and relatively high capacity for H_2 and CO_2 adsorption but displays a lower activity than CuZnZr (C3Z2Z5). This suggests the Cu surface area is not the exclusive factor in determining the catalyst activity for CO_2 hydrogenation to methanol. Moreover, CuZr is more active than CuZn, indicating more effective active sites formed on CuZr. Based on the CO_2-TPD results, the presence of the Cu-ZrO_2 interface can effectively increase the CO_2 adsorption capacity, thereby promoting the reaction. We consider that both ZnO and ZrO_2 play an important role in working with Cu for the construction of the active sites over CuZnZr. As indicated by the XRD and TEM analyses, CuZn alloy is formed from strong Cu-ZnO interaction over C3Z2Z5. The C3Z2Z5 catalyst exhibits a higher capacity for CO_2 adsorption relative to CuZn and CuZr, implying the involvement of the Cu-ZrO_2 interface in catalyzing the reaction. It is possible that the cooperation between Cu-oxide interaction (e.g., CuZn alloy and Cu-ZrO_2

interface) acts as the active sites, effectively improving carbon dioxide conversion rate and methanol selectivity. Since the composition of ZnO and ZrO_2 impacts the Cu-oxide interaction, the following work further investigates the optimization of ZnO and ZrO_2 contents and establishes the relationship between the catalyst structure and the activity.

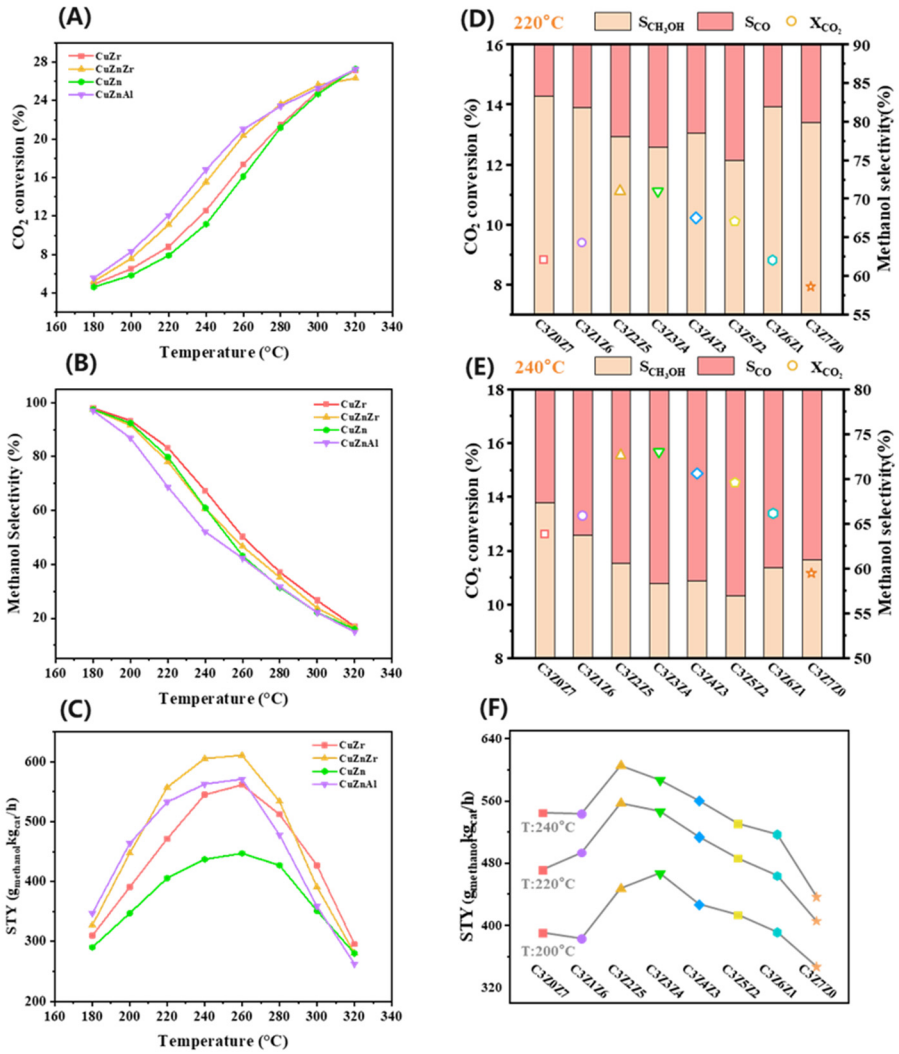

Figure 7. (**A**) CO_2 conversion, (**B**) methanol selectivity, (**C**) STY of methanol of CuZn, CuZr, CuZnZr, and commercial CuZnAl catalysts. The variation of CO_2 conversion, product selectivity in the reaction at (**D**) 220 °C and (**E**) 240 °C, and (**F**) STY of methanol for all catalysts. (P = 3 MPa, GHSV = 18,000 mL/g_{cat}/h).

The effect of varying ZnO/ZrO_2 ratios on the catalytic performance in the reaction over $Cu/ZnO/ZrO_2$ at 220 °C and 240 °C reveals the highest CO_2 conversion is achieved at the ZnO/ZrO_2 ratio of 2:5 to 3:4 (Figure 7D,E), suggesting an optimized content of ZnO and ZrO_2 is required for efficient activation and conversion of CO_2. The methanol selectivity does not vary dramatically with changes in the ZnO/ZrO_2 ratio. Due to the larger change in CO_2 conversion than in methanol selectivity, the overall trend of STY of methanol with the Zn/Zr ratio is similar to the trend of CO_2 conversion (Figure 7F). Except for 220 °C, the STY of methanol of C3Z2Z5 is the highest at all other temperatures. The trend of activity variation is similar to the results of Zn LMM and CO_2-TPD. The catalyst activity increased before the ZnO content increased to 20%, possibly due to the increase in CuZn alloy content. However, as the ZnO content increases, the ZrO_2 content correspondingly decreases, and the Cu-ZrO_2 interface gradually decreases, which may lead to a decrease in catalyst activity.

In C3Z2Z5, the amount of CuZn alloy and Cu-ZrO_2 interface reach the highest values, demonstrating the best catalytic activity.

The C3Z2Z5 catalyst was used to investigate the effect of reduction temperature on catalytic performance (Figure 8). When the reduction temperature exceeds 260 °C, there is no significant difference in CO_2 conversion, methanol selectivity, and STY of methanol (Figure 8A–C), indicating that the catalyst had been completely reduced beyond 260 °C, which is consistent with the results of H_2-TPR. Under the reaction conditions of 220, 240, and 260 °C, with the increase in reduction temperature, the conversion rate slightly increases and then remains unchanged, while the selectivity initially increases and then decreases (Figure 8D–F). When the reduction temperature is higher than 260 °C, the catalytic performance does not change significantly, indicating that a higher reduction temperature below 300 °C does not significantly alter the structure of the catalyst. The C3Z2Z5 catalyst was also selected to investigate the impact of gas hourly space velocity (GHSV, 6000, 12,000, 18,000, and 24,000 mL/g_{cat}/h) on catalytic performance (Figure 9). Lower GHSV results in higher CO_2 conversion but lower methanol selectivity, indicating that low GHSV is more conducive to the production of CO through the RWGS. The STY of methanol is also increased with the increase of GHSV, reaching a maximum value at 24,000 mL/g_{cat}/h under the conditions used here.

In the long-term stability test for 110 h (P = 3 MPa, T = 240 °C, GHSV = 18,000 mL/g_{cat}/h), the CO_2 conversion and methanol selectivity over the C3Z2Z5 catalyst remain basically unchanged (Figure S4), and exhibit no significant deactivation. Comparing the XRD patterns of the catalyst after reduction and after 110 h reaction (Figure S4B), the intensities of the Cu peak (2θ = 43.3° and 50.4°) are similar, indicating that the C3Z2Z5 sample after 110 h reaction exhibits no severe sintering of Cu particles. TEM and EDS mapping of the spent catalyst (Figure S4C–F) verify that the long-term stability test does not cause aggregation of the Cu particles, indicating that the C3Z2Z5 catalyst exhibits good stability.

The adsorption capacity of catalysts on reactants will have a significant impact on the reaction performance. When the metal Cu content is fixed, except for the Cu/ZnO catalyst, there is not much difference in the H_2 adsorption amount, but the change in the CO_2 adsorption amount is more significant. The correlation analysis between the CO_2 desorption amount and catalyst performance (Figure 10A) shows that the catalytic activity is directly proportional to the CO_2 desorption amount, indicating that the ZnO/ZrO_2 ratio affects the reaction performance by adjusting the CO_2 adsorption sites. When the ZnO/ZrO_2 ratio is 2:5, the number of strong basic sites on the catalyst surface is the highest, effectively improving the CO_2 adsorption amount and enhancing the catalytic activity.

XRD, HR-TEM, and XPS analyses show that a fraction of ZnO is reduced to Zn^0 and reacts with metallic Cu to form a CuZn alloy. The content of Zn^0 in different samples can be calculated by Zn-LMM, which corresponds to the amount of CuZn alloy. By correlating the catalytic performance with the content of Zn^0 (Figure 10B), C3Z2Z5 with the highest CuZn alloy content exhibits the highest activity, while the catalysts with lower Zn^0 content also had lower catalytic performance, indicating that the presence of CuZn alloy effectively promotes the reaction. The change in the ZnO/ZrO_2 ratio not only affects the amount of CuZn alloy but also affects the number of Cu-ZrO_2 interfaces, thereby affecting the adsorption capacity of CO_2. C3Z4Z3 and C3Z3Z4 have similar CuZn alloy content, but C3Z3Z4 exhibits better catalytic activity, which can be associated with an increase in the CO_2 adsorption capacity. Thus, we consider the oxide (ZnO and ZrO_2) composition mainly affects the catalytic performance in methanol synthesis by regulating the quantity of CuZn alloys and Cu-ZrO_2 interaction, and furthers the ability for adsorption/activation of reactants. The synergistic sites associated with the CuZn alloy and Cu-ZrO_2 interface in the optimized Cu/ZnO/ZrO_2 catalyst (C3Z2Z5) reach the maximum, contributing to the enhanced production of methanol.

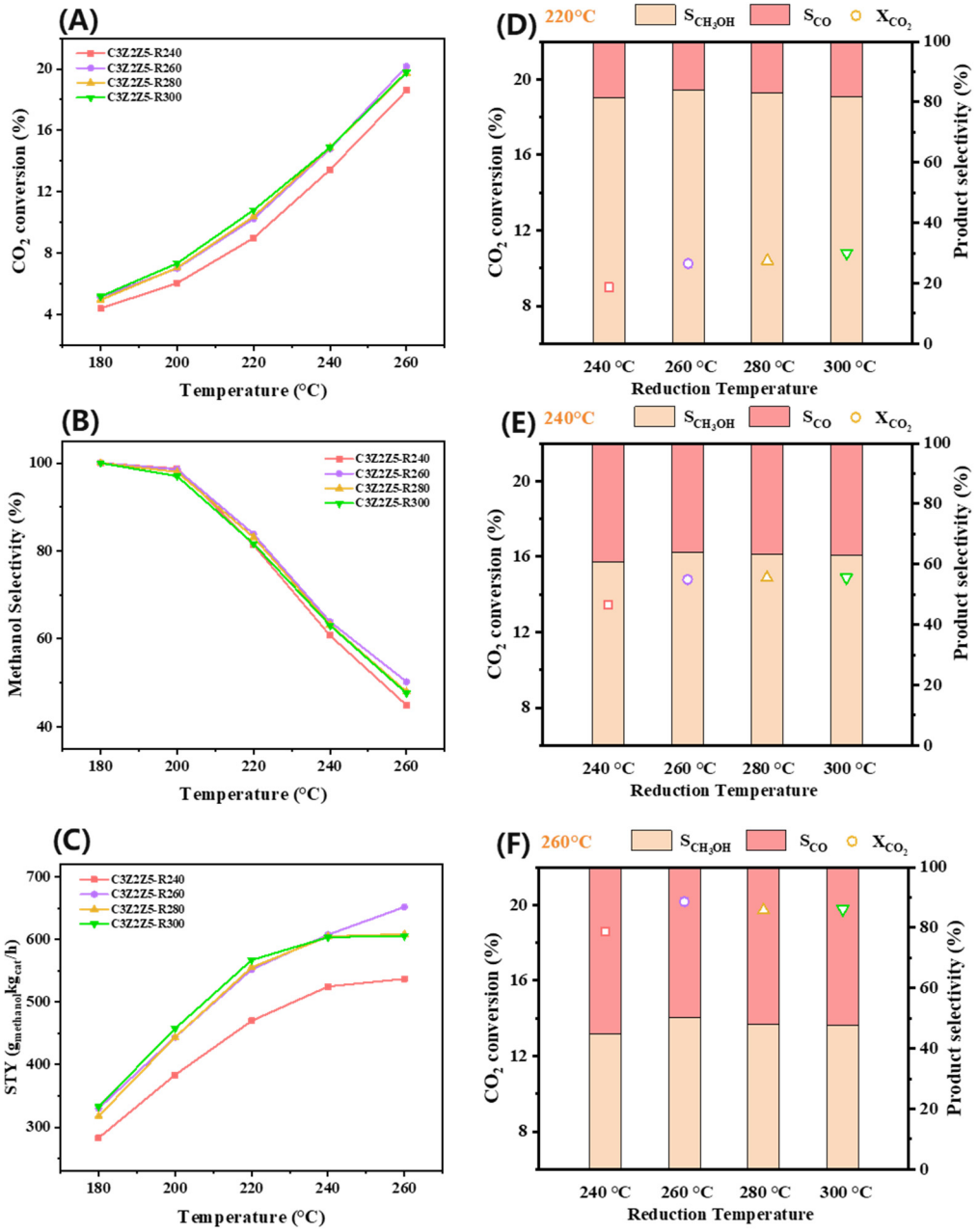

Figure 8. (**A**) CO_2 conversion, (**B**) methanol selectivity, (**C**) STY of methanol of C3Z2Z5 at different reduction temperatures, the variation of CO_2 conversion, product selectivity in the reaction at (**D**) 220 °C, (**E**) 240 °C, and (**F**) 260 °C at different reduction temperatures (P = 3 MPa, GHSV = 18,000 mL/g_{cat}/h).

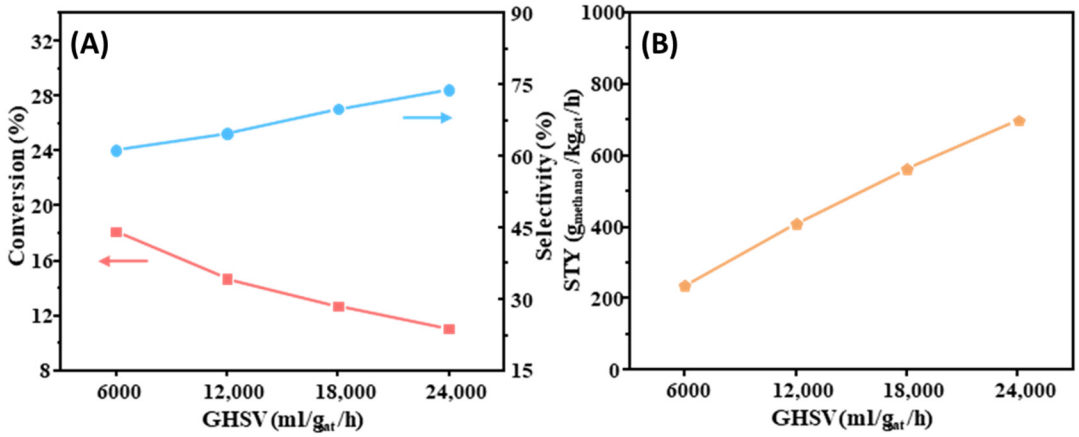

Figure 9. (**A**) CO_2 conversion and methanol selectivity, (**B**) STY of methanol of C3Z2Z5 at different GHSV (P = 3 MPa, T = 240 °C).

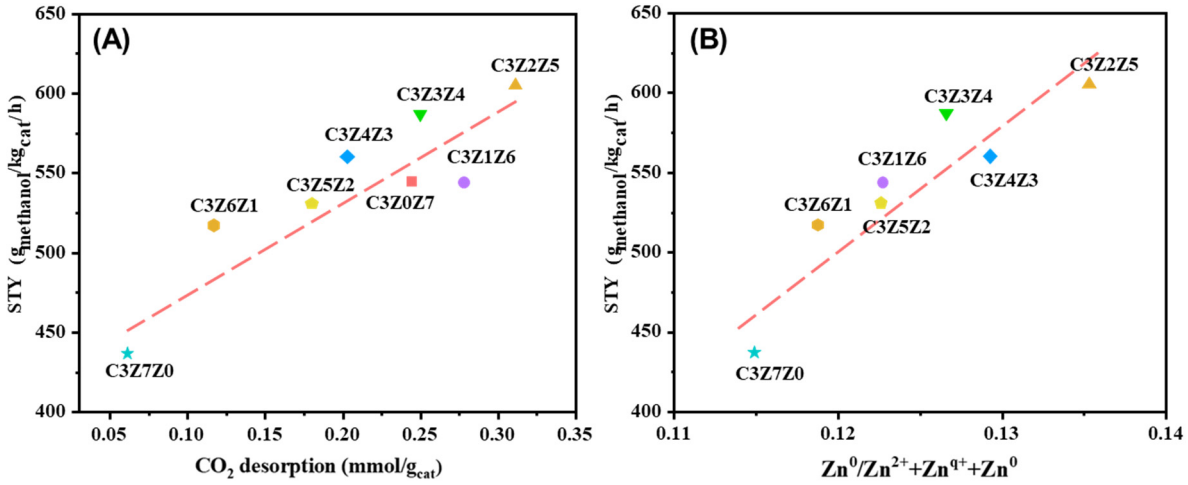

Figure 10. Relationship between STY of methanol (P = 3 MPa, T = 240 °C, GHSV = 18,000 mL/g_{cat}/h) and (**A**) CO_2 desorption amount, (**B**) Zn^0 content.

3. Materials and Methods

3.1. Catalyst Preparation

A series of $Cu/ZnO/ZrO_2$ catalysts with varying Cu contents were prepared by coprecipitation. The mixed nitrates (including copper nitrate, zinc nitrate, and zirconium nitrate) in ethanol were precipitated at 70 °C using excess oxalic acid under stirring for 1 h, then aged for 4 h at room temperature. The precipitate was separated by centrifugation, washed three times with ethanol, and dried at 80 °C for 12 h. The dried samples were calcined at 450 °C for 4 h. After calcination, the samples were subjected to compression, crushing, and sieving treatment and 40–60 mesh particles were selected for the catalysts test. The target mass fraction of Cu was fixed at 30 wt%, and a total of 8 samples were prepared by sequentially adjusting the mass ratio of ZnO/ZrO_2. The calcined catalysts were named based on element content.

3.2. Catalyst Characterization

Nitrogen physisorption was tested using a Micromeritics ASAP 2460 (Micromeritics instrument Ltd., Atlanta, America) system for analysis of the specific surface area (S_{BET}) and pore structure (pore volume and pore size) according to the standard Braeuer–Emmett–Teller (BET) method and Barrett–Joyner–Halenda desorption branch. All the samples were outgassed under vacuum at 300 °C for 4 h before the nitrogen physisorption test.

XRD patterns of both calcined and reduced samples were carried out by using a Rigaku D/MAX 2500 X-ray diffractometer (Rigaku Corporation, Tokyo, Japan) using Cu Kα radiation (λ = 1.542 Å), and the results were analyzed using JADE6 (V6.5.26@07/02/05). All samples were measured over the range of $20^\circ \leq 2\theta \leq 80^\circ$ with a step size of 0.02° at ambient temperature.

TEM and HAADF-STEM (high-angle annular dark-field scanning transmission electron microscopy) were used to observe the morphology of all the samples, which were tested by using a JEM-2100F electron microscope equipped with an EDX spectrometer (JEOL, Tokyo, Japan), and the obtained images were analyzed with a Gatan Digital Micrograph. All samples were sonicated in an ethanol solution and then dropped onto a holey carbon/Mo grid before measurements.

ICP-OES was used to measure the actual content of Cu, Zn, and Zr by using Vista-MPX (Agilent, Palo Alto, America). A certain mass of catalyst was dissolved in hydrofluoric acid, and the resultant solution was diluted using boric acid. The diluted solution was injected into the instrument through a peristaltic pump, and the average value of each element content was measured three times to reduce the error. The characteristic wavelengths selected for Cu, Zn, and Zr elements are 327.395 nm, 213.857 nm, and 349.619 nm.

XPS were obtained to analyze the valence states of surface elements by using a Thermo K-Alpha+ system (Thermo Fisher Scientific, Waltham, America), and Al Kα (E = 1486.6 eV) was applied for exciting the photoelectron spectra under ultra-high vacuum (6.67×10^{-7} Pa). All the binding energy was calibrated by C1s (284.6 eV), and the results were analyzed using Avantage software (V5.9921).

H_2-TPR, H_2-TPD, CO_2-TPD, and N_2O titration were conducted using a Micromeritics Chemisorb 2920 system (Micromeritics instrument Ltd., Atlanta, America). Subsequently, 50 mg of catalyst was loaded into a quartz U-tube and pretreated in Ar at 200 °C for 1 h to remove adsorbed water. After the pretreatment, samples were cooled to 30 °C, subjected to 10% H_2/Ar (10 mL/min), and heated to 300 °C at 10 °C/min. For H_2 chemisorption, the reduced samples were cooled to 200 °C, purged in Ar for 30 min, and subjected to 10% H_2/Ar (10 mL/min) for pulse titration until saturation. Following H_2 chemisorption, the samples were cooled to 30 °C and heated from 30 °C to 800 °C at a rate of 10 °C/min in Ar for H_2-TPD analysis. For the CO_2-TPD analysis, the reduced samples were purged in He at 300 °C for 30 min, cooled to 30 °C, subjected to 10% CO_2/He (30 mL/min) for 1 h for CO_2 adsorption, and heated to 800 °C at 10 °C/min in He. N_2O titration was used to measure the exposed metal Cu surface area. The samples were reduced as mentioned above, purged in Ar at 300 °C for 30 min, cooled to 30 °C, and subjected to N_2O titration at 30 °C for 30 min. The samples were purged in Ar again to remove the physisorbed N_2O and heated to 300 °C, subjected to 10% H_2/Ar (10 mL/min) for H_2 titration until saturated. All the signals were recorded by a TCD (thermal conductivity detector). The D_{Cu}, S_{Cu}, and d_{Cu} were calculated according to the following equations:

$$N_{Cu_0} = \frac{2n_{H_2}}{m_{cat}} \quad (3)$$

$$D_{Cu} = \frac{N_{Cu_0} M_{Cu}}{W_{Cu}} \quad (4)$$

$$S_{Cu_0} = \frac{N_{Cu_0} N_A}{S_{D_{Cu}}} \quad (5)$$

$$d_{Cu} = \frac{6M_{Cu}}{D_{Cu} \rho \sigma N_A} \quad (6)$$

where M_{Cu} is the atomic weight of copper, W_{Cu} is the Cu content determined by ICP-OES, S_{DCu} is the copper surface density (1.47×10^{19} atoms/m^2), ρ is the copper metal density (8.94 g/cm^3), and σ is the area occupied by a surface copper atom (6.85 Å^2/atom).

For ex situ characterizations (including nitrogen physisorption, XRD, TEM, and XPS), the calcined catalyst should be reduced at 300 °C for 3 h.

3.3. Catalyst Testing

The catalytic performance was evaluated using a fixed-bed continuous-flow stainless-steel reactor. The catalyst (100 mg, 40−60 mesh) was reduced in H_2 (10 mL/min) for 3 h before the reaction and cooled down to 180 °C, which was monitored by a thermocouple in the catalyst bed. Afterward, the hydrogen gas was turned off and the feed gases (CO_2/H_2 = 3/1) and N_2 (internal standard) were introduced, increasing the pressure to 3 MPa. Next, the reactor temperature was raised to the test temperature (180–300 °C). The composition of the outlet gas was analyzed online using a gas chromatographic system (Shimadzu, GC-2014) equipped with an FID (flame ionization detector, for methanol) and a TCD (thermal conductivity detector, for N_2, CO_2, CO, and CH_4). The X_{CO_2} (conversion of CO_2), S_{CH3OH} (methanol selectivity), and STY_{CH3OH} (space-time yield of methanol) were calculated with the following equations:

$$X_{CO_2} = \frac{F_{(CO)out} + F_{(CH_3OH)out}}{F_{(CO_2)out} + F_{(CO)out} + F_{(CH_3OH)out}} \times 100\% \quad (7)$$

$$S_{CH_3OH} = \frac{F_{(CH_3OH)out}}{F_{(CO)out} + F_{(CH_3OH)out}} \times 100\% \quad (8)$$

$$STY_{CH_3OH} = \frac{F_{(CO_2)in} \cdot X_{CO_2} \cdot S_{CH_3OH} \cdot M_{CH_3OH}}{22.4 \cdot m} \quad (9)$$

where F is the volumetric flow rate, M_{CH3OH} is the molecule weight of methanol, and m_{cat} refers to the mass of the catalyst. The deviation of the carbon balance is within 5%.

4. Conclusions

This study has established the effect of ZnO and ZrO_2 contents on the $Cu/ZnO/ZrO_2$ catalyst structure/surface characteristics and catalytic performance in the CO_2 hydrogenation to methanol. CuZn alloy was formed in the catalyst containing ZnO, and the ZnO/ZrO_2 ratio can affect the content of CuZn alloy. A correlation between the amount of CuZn alloy and the catalytic activity reveals the participation of CuZn alloy in the reaction. The ZnO/ZrO_2 ratio also affects the amount of strong basic sites on the catalyst surface. With an increase in strong basic sites related to the Cu-ZrO_2 interfaces, the amount of CO_2 desorption significantly increases. The increase in both CuZn alloy content and Cu-ZrO_2 interfaces promotes the process of CO_2 hydrogenation to methanol. The optimized catalyst C3Z2Z5 shows the highest STY of methanol (610.8 $g_{CH3OH}/kg_{cat}/h$) with no significant decrease in activity during long-term stability testing.

Supplementary Materials: The following supporting information can be downloaded at: https://www.mdpi.com/article/10.3390/catal13101337/s1, Figure S1: N_2 adsorption-desorption isotherms (A) and pore size distributions (B); Figure S2: TEM images of reduced catalysts; Figure S3: EDS-mapping images of reduced catalysts; Figure S4: C3Z2Z5 (A) 110 h stability test, (B) XRD pattern after reduction and stability test, TEM image (C) after reduction and (D) stability test, EDS-mapping images (E) after reduction and (F) stability test; Table S1: Catalytic performance of Cu-based catalysts for CO_2 hydrogenation to methanol [49–59].

Author Contributions: Conceptualization and methodology, X.C., X.Z., M.L. and X.M.; investigation, X.C., X.Z., X.H., J.C., Z.H., Z.Z., H.Z. and P.G.; data curation, X.C., X.Z. and M.L.; writing—original draft, X.C. and X.Z.; writing—review and editing, X.C., X.Z. and M.L.; supervision, M.L., J.L. (Jing Lv), and X.M.; project administration, J.L. (Jing Li), F.L. and X.M. All authors have read and agreed to the published version of the manuscript.

Funding: This research was funded by National Natural Science Foundation of China (22178265, U21B2096, 21938008) and Tianjin Natural Science and Technology Project (21JCYBJC00400).

Data Availability Statement: The original data are available from X.C., X.Z. and M.L.

Acknowledgments: The authors acknowledge the financial support by National Natural Science Foundation of China (22178265, U21B2096, 21938008), Tianjin Natural Science and Technology Project (21JCYBJC00400) and Beijing Building Materials Academy of Science Research.

Conflicts of Interest: The funders had no role in the design of the study; in the collection, analyses, or interpretation of data; in the writing of the manuscript; or in the decision to publish the results.

References

1. Alwin, M.; Mathias, P. Synthetic Manufacture of Methanol. U.S. Patent No. 1,569,775, 12 January 1926.
2. Cifre, P.G.; Badr, O. Renewable hydrogen utilisation for the production of methanol. *Energy Convers. Manag.* **2007**, *48*, 519–527. [CrossRef]
3. Shih, C.F.; Zhang, T.; Li, J.; Bai, C. Powering the future with liquid sunshine. *Joule* **2018**, *2*, 1925–1949. [CrossRef]
4. Wang, Z.-Q.; Xu, Z.-N.; Peng, S.-Y.; Zhang, M.-J.; Lu, G.; Chen, Q.-S.; Chen, Y.; Guo, G.-C. High-performance and long-lived Cu/SiO_2 nanocatalyst for CO_2 hydrogenation. *ACS Catal.* **2015**, *5*, 4255–4259. [CrossRef]
5. Arena, F.; Italiano, G.; Barbera, K.; Bordiga, S.; Bonura, G.; Spadaro, L.; Frusteri, F. Solid-state interactions, adsorption sites and functionality of Cu-ZnO/ZrO_2 catalysts in the CO_2 hydrogenation to CH_3OH. *Appl. Catal. A Gen.* **2008**, *350*, 16–23. [CrossRef]
6. Dong, X.; Li, F.; Zhao, N.; Xiao, F.; Wang, J.; Tan, Y. CO_2 hydrogenation to methanol over $Cu/ZnO/ZrO_2$ catalysts prepared by precipitation-reduction method. *Appl. Catal. B Environ.* **2016**, *191*, 8–17. [CrossRef]
7. Nakamura, J.; Uchijima, T.; Kanai, Y.; Fujitani, T. The role of ZnO in Cu/ZnO methanol synthesis catalysts. *Catal. Today* **1996**, *28*, 223–230. [CrossRef]
8. Kattel, S.; Ramírez, P.J.; Chen, J.G.; Rodriguez, J.A.; Liu, P. Active sites for CO_2 hydrogenation to methanol on Cu/ZnO catalysts. *Science* **2017**, *355*, 1296–1299. [CrossRef]
9. Fujitani, T.; Nakamura, J. The chemical modification seen in the Cu/ZnO methanol synthesis catalysts. *Appl. Catal. A Gen.* **2000**, *191*, 111–129. [CrossRef]
10. Lunkenbein, T.; Schumann, J.; Behrens, M.; Schlögl, R.; Willinger, M.G. Formation of a ZnO overlayer in industrial $Cu/ZnO/Al_2O_3$ catalysts induced by strong metal–support interactions. *Angew. Chem.* **2015**, *127*, 4627–4631. [CrossRef]
11. Kuld, S.; Thorhauge, M.; Falsig, H.; Elkjær, C.F.; Helveg, S.; Chorkendorff, I.; Sehested, J. Quantifying the promotion of Cu catalysts by ZnO for methanol synthesis. *Science* **2016**, *352*, 969–974. [CrossRef]
12. Behrens, M.; Studt, F.; Kasatkin, I.; Kühl, S.; Hävecker, M.; Abild-Pedersen, F.; Zander, S.; Girgsdies, F.; Kurr, P.; Kniep, B.-L. The active site of methanol synthesis over $Cu/ZnO/Al_2O_3$ industrial catalysts. *Science* **2012**, *336*, 893–897. [CrossRef]
13. Bansode, A.; Tidona, B.; von Rohr, P.R.; Urakawa, A. Impact of K and Ba promoters on CO_2 hydrogenation over Cu/Al_2O_3 catalysts at high pressure. *Catal. Sci. Technol.* **2013**, *3*, 767–778. [CrossRef]
14. Noh, G.; Lam, E.; Alfke, J.L.; Larmier, K.; Searles, K.; Wolf, P.; Copéret, C. Selective hydrogenation of CO_2 to CH_3OH on supported Cu nanoparticles promoted by isolated Ti^{IV} surface sites on SiO_2. *ChemSusChem* **2019**, *12*, 968–972. [CrossRef]
15. Hartadi, Y.; Widmann, D.; Behm, R.J. CO_2 hydrogenation to methanol on supported Au catalysts under moderate reaction conditions: Support and particle size effects. *ChemSusChem* **2015**, *8*, 456–465. [CrossRef]
16. Yang, X.; Kattel, S.; Senanayake, S.D.; Boscoboinik, J.A.; Nie, X.; Graciani, J.; Rodriguez, J.A.; Liu, P.; Stacchiola, D.J.; Chen, J.G. Low pressure CO_2 hydrogenation to methanol over gold nanoparticles activated on a CeO_x/TiO_2 interface. *J. Am. Chem. Soc.* **2015**, *137*, 10104–10107. [CrossRef]
17. Köppel, R.A.; Stöcker, C.; Baiker, A. Copper-and silver–zirconia aerogels: Preparation, structural properties and catalytic behavior in methanol synthesis from carbon dioxide. *J. Catal.* **1998**, *179*, 515–527. [CrossRef]
18. Collins, S.E.; Baltanas, M.A.; Bonivardi, A.L. An infrared study of the intermediates of methanol synthesis from carbon dioxide over $Pd/\beta\text{-}Ga_2O_3$. *J. Catal.* **2004**, *226*, 410–421. [CrossRef]
19. Jiang, X.; Koizumi, N.; Guo, X.; Song, C. Bimetallic Pd–Cu catalysts for selective CO_2 hydrogenation to methanol. *Appl. Catal. B Environ.* **2015**, *170*, 173–185. [CrossRef]
20. Bahruji, H.; Bowker, M.; Hutchings, G.; Dimitratos, N.; Wells, P.; Gibson, E.; Jones, W.; Brookes, C.; Morgan, D.; Lalev, G. Pd/ZnO catalysts for direct CO_2 hydrogenation to methanol. *J. Catal.* **2016**, *343*, 133–146. [CrossRef]
21. Bai, S.; Shao, Q.; Feng, Y.; Bu, L.; Huang, X. Highly efficient carbon dioxide hydrogenation to methanol catalyzed by zigzag platinum–cobalt nanowires. *Small* **2017**, *13*, 1604311. [CrossRef]
22. Martin, O.; Martín, A.J.; Mondelli, C.; Mitchell, S.; Segawa, T.F.; Hauert, R.; Drouilly, C.; Curulla-Ferré, D.; Pérez-Ramírez, J. Indium oxide as a superior catalyst for methanol synthesis by CO_2 hydrogenation. *Angew. Chem.* **2016**, *128*, 6369–6373. [CrossRef]
23. Chen, T.-Y.; Cao, C.; Chen, T.-B.; Ding, X.; Huang, H.; Shen, L.; Cao, X.; Zhu, M.; Xu, J.; Gao, J. Unraveling highly tunable selectivity in CO_2 hydrogenation over bimetallic In-Zr oxide catalysts. *ACS Catal.* **2019**, *9*, 8785–8797. [CrossRef]
24. Men, Y.-L.; Liu, Y.; Wang, Q.; Luo, Z.-H.; Shao, S.; Li, Y.-B.; Pan, Y.-X. Highly dispersed Pt-based catalysts for selective CO_2 hydrogenation to methanol at atmospheric pressure. *Chem. Eng. Sci.* **2019**, *200*, 167–175. [CrossRef]
25. Shen, C.; Sun, K.; Zhang, Z.; Rui, N.; Jia, X.; Mei, D.; Liu, C.-J. Highly active Ir/In_2O_3 catalysts for selective hydrogenation of CO_2 to methanol: Experimental and theoretical studies. *ACS Catal.* **2021**, *11*, 4036–4046. [CrossRef]

26. Zhong, J.; Yang, X.; Wu, Z.; Liang, B.; Huang, Y.; Zhang, T. State of the art and perspectives in heterogeneous catalysis of CO_2 hydrogenation to methanol. *Chem. Soc. Rev.* **2020**, *49*, 1385–1413. [CrossRef]
27. Kuld, S.; Conradsen, C.; Moses, P.G.; Chorkendorff, I.; Sehested, J. Quantification of zinc atoms in a surface alloy on copper in an industrial-type methanol synthesis catalyst. *Angew. Chem. Int. Ed.* **2014**, *53*, 5941–5945. [CrossRef]
28. Tisseraud, C.; Comminges, C.; Belin, T.; Ahouari, H.; Soualah, A.; Pouilloux, Y.; Le Valant, A. The Cu–ZnO synergy in methanol synthesis from CO_2, Part 2: Origin of the methanol and CO selectivities explained by experimental studies and a sphere contact quantification model in randomly packed binary mixtures on Cu–ZnO coprecipitate catalysts. *J. Catal.* **2015**, *330*, 533–544. [CrossRef]
29. Chang, X.; Han, X.; Pan, Y.; Hao, Z.; Chen, J.; Li, M.; Lv, J.; Ma, X. Insight into the Role of Cu–ZrO_2 Interaction in Methanol Synthesis from CO_2 Hydrogenation. *Ind. Eng. Chem. Res.* **2022**, *61*, 6872–6883. [CrossRef]
30. Natesakhawat, S.; Lekse, J.W.; Baltrus, J.P.; Ohodnicki, P.R., Jr.; Howard, B.H.; Deng, X.; Matranga, C. Active sites and structure–activity relationships of copper-based catalysts for carbon dioxide hydrogenation to methanol. *ACS Catal.* **2012**, *2*, 1667–1676. [CrossRef]
31. Cargnello, M.; Doan-Nguyen, V.V.; Gordon, T.R.; Diaz, R.E.; Stach, E.A.; Gorte, R.J.; Fornasiero, P.; Murray, C.B. Control of metal nanocrystal size reveals metal-support interface role for ceria catalysts. *Science* **2013**, *341*, 771–773. [CrossRef]
32. Zhang, Z.; Jing, M.; Chen, H.; Okejiri, F.; Liu, J.; Leng, Y.; Liu, H.; Song, W.; Hou, Z.; Lu, X. Transfer hydrogenation of fatty acids on Cu/ZrO_2: Demystifying the role of carrier structure and metal–support interface. *ACS Catal.* **2020**, *10*, 9098–9108. [CrossRef]
33. Yu, J.; Yang, M.; Zhang, J.; Ge, Q.; Zimina, A.; Pruessmann, T.; Zheng, L.; Grunwaldt, J.-D.; Sun, J. Stabilizing Cu^+ in Cu/SiO_2 catalysts with a shattuckite-like structure boosts CO_2 hydrogenation into methanol. *ACS Catal.* **2020**, *10*, 14694–14706. [CrossRef]
34. Feng, Y.; Li, Z.; Liu, H.; Dong, C.; Wang, J.; Kulinich, S.A.; Du, X. Laser-prepared CuZn alloy catalyst for selective electrochemical reduction of CO_2 to ethylene. *Langmuir* **2018**, *34*, 13544–13549. [CrossRef] [PubMed]
35. Yuan, L.; Wang, C.; Cai, R.; Wang, Y.; Zhou, G. Spontaneous ZnO nanowire formation during oxidation of Cu-Zn alloy. *J. Appl. Phys.* **2013**, *114*, 023512. [CrossRef]
36. Li, K.; Chen, J.G. CO_2 hydrogenation to methanol over ZrO_2-containing catalysts: Insights into ZrO_2 induced synergy. *ACS Catal.* **2019**, *9*, 7840–7861. [CrossRef]
37. Wang, Y.; Kattel, S.; Gao, W.; Li, K.; Liu, P.; Chen, J.G.; Wang, H. Exploring the ternary interactions in Cu–ZnO–ZrO_2 catalysts for efficient CO_2 hydrogenation to methanol. *Nat. Commun.* **2019**, *10*, 1166. [CrossRef]
38. Frei, E.; Gaur, A.; Lichtenberg, H.; Zwiener, L.; Scherzer, M.; Girgsdies, F.; Lunkenbein, T.; Schlögl, R. Cu−Zn alloy formation as unfavored state for efficient methanol catalysts. *ChemCatChem* **2020**, *12*, 4029–4033. [CrossRef]
39. Witoon, T.; Chalorngtham, J.; Dumrongbunditkul, P.; Chareonpanich, M.; Limtrakul, J. CO_2 hydrogenation to methanol over Cu/ZrO_2 catalysts: Effects of zirconia phases. *Chem. Eng. J.* **2016**, *293*, 327–336. [CrossRef]
40. Liang, Z.-Q.; Zhuang, T.-T.; Seifitokaldani, A.; Li, J.; Huang, C.-W.; Tan, C.-S.; Li, Y.; De Luna, P.; Dinh, C.T.; Hu, Y. Copper-on-nitride enhances the stable electrosynthesis of multi-carbon products from CO_2. *Nat. Commun.* **2018**, *9*, 3828. [CrossRef]
41. Rather, R.A.; Singh, S.; Pal, B. A Cu^{+1}/Cu^0-TiO_2 mesoporous nanocomposite exhibits improved H_2 production from H_2O under direct solar irradiation. *J. Catal.* **2017**, *346*, 1–9. [CrossRef]
42. Wang, W.; Qu, Z.; Song, L.; Fu, Q. An investigation of Zr/Ce ratio influencing the catalytic performance of CuO/$Ce_{1-x}Zr_xO_2$ catalyst for CO_2 hydrogenation to CH_3OH. *J. Energy Chem.* **2020**, *47*, 18–28. [CrossRef]
43. Gao, P.; Li, F.; Zhan, H.; Zhao, N.; Xiao, F.; Wei, W.; Zhong, L.; Wang, H.; Sun, Y. Influence of Zr on the performance of Cu/Zn/Al/Zr catalysts via hydrotalcite-like precursors for CO_2 hydrogenation to methanol. *J. Catal.* **2013**, *298*, 51–60. [CrossRef]
44. Choi, E.; Song, K.; An, S.; Lee, K.; Youn, M.; Park, K.; Jeong, S.; Kim, H. Cu/ZnO/AlOOH catalyst for methanol synthesis through CO_2 hydrogenation. *Korean J. Chem. Eng.* **2018**, *35*, 73–81. [CrossRef]
45. Gao, P.; Li, F.; Zhao, N.; Xiao, F.; Wei, W.; Zhong, L.; Sun, Y. Influence of modifier (Mn, La, Ce, Zr and Y) on the performance of Cu/Zn/Al catalysts via hydrotalcite-like precursors for CO_2 hydrogenation to methanol. *Appl. Catal. A Gen.* **2013**, *468*, 442–452. [CrossRef]
46. Han, X.; Li, M.; Chang, X.; Hao, Z.; Chen, J.; Pan, Y.; Kawi, S.; Ma, X. Hollow structured Cu@ZrO_2 derived from Zr-MOF for selective hydrogenation of CO_2 to methanol. *J. Energy Chem.* **2022**, *71*, 277–287. [CrossRef]
47. Zhao, H.B.; Yu, R.F.; Ma, S.C.; Xu, K.Z.; Chen, Y.; Jiang, K.; Fang, Y.; Zhu, C.X.; Liu, X.C.; Tang, Y.; et al. The role of Cu_1-O_3 species in single-atom Cu/ZrO_2 catalyst for CO_2 hydrogenation. *Nat. Catal.* **2022**, *5*, 818–831. [CrossRef]
48. Choi, Y.; Futagami, K.; Fujitani, T.; Nakamura, J. The role of ZnO in Cu/ZnO methanol synthesis catalysts—Morphology effect or active site model? *Appl. Catal. A Gen.* **2001**, *208*, 163–167. [CrossRef]
49. Lam, E.; Larmier, K.; Wolf, P.; Tada, S.; Safonova, O.V.; Coperet, C. Isolated Zr surface sites on silica promote hydrogenation of CO_2 to CH_3OH in supported Cu catalysts. *J. Am. Chem. Soc.* **2018**, *140*, 10530–10535. [CrossRef]
50. Larmier, K.; Liao, W.C.; Tada, S.; Lam, E.; Verel, R.; Bansode, A.; Urakawa, A.; Comas-Vives, A.; Coperet, C. CO_2-to-methanol hydrogenation on zirconia-supported copper nanoparticles: Reaction intermediates and the role of the metal-support interface. *Angew. Chem. Int. Ed.* **2017**, *56*, 2318–2323. [CrossRef]
51. Tada, S.; Fujiwara, K.; Yamamura, T.; Nishijima, M.; Uchida, S.; Kikuchi, R. Flame spray pyrolysis makes highly loaded Cu nanoparticles on ZrO_2 for CO_2-to-methanol hydrogenation. *Chem. Eng. J.* **2020**, *381*, 122750. [CrossRef]
52. Shohei, T.; Shingo, K.; Tetsuo, H.; Hiromu, K.; Akane, N.; Kenichi, K.; Takashi, T.; Ken-Ichi, S.; Shigeo, S. Design of interfacial sites between Cu and amorphous ZrO_2 dedicated to CO_2-to-methanol hydrogenation. *ACS Catal.* **2018**, *8*, 7809–7819.

53. Amenomiya, Y. Methanol synthesis from CO_2 + H_2 II. Copper-based binary and ternary catalysts. *Appl. Catal.* **1987**, *30*, 57–68. [CrossRef]
54. Haowang, Y.; Guigao, W.; Wang, H.; Zheng, Y.E.; Na, W.; Zhaili, K. Structure–activity relationships of Cu–ZrO_2 catalysts for CO_2 hydrogenation to methanol: Interaction effects and reaction mechanism. *RSC Adv.* **2017**, *7*, 8709–8717.
55. Guo, X.; Mao, D.; Lu, G.; Wang, S.; Wu, G. Glycine–nitrate combustion synthesis of CuO–ZnO–ZrO_2 catalysts for methanol synthesis from CO_2 hydrogenation. *J. Catal.* **2010**, *271*, 178–185. [CrossRef]
56. Sánchez-Contador, M.; Ateka, A.; Rodriguez-Vega, P.; Bilbao, J.; Aguayo, A.T. Optimization of the Zr content in the CuO-ZnO-ZrO_2 /SAPO-11 catalyst for the selective hydrogenation of CO+CO_2 mixtures in the direct synthesis of dimethyl ether. *Ind. Eng. Chem. Res.* **2018**, *57*, 1169–1178. [CrossRef]
57. Arena, F.; Mezzatesta, G.; Zafarana, G.; Trunfio, G.; Frusteri, F.; Spadaro, L. Effects of oxide carriers on surface functionality and process performance of the Cu–ZnO system in the synthesis of methanol via CO_2 hydrogenation. *J. Catal.* **2013**, *300*, 141–151. [CrossRef]
58. Ramli, M.Z.; Syed-Hassan, S.S.A.; Hadi, A. Performance of Cu-Zn-Al-Zr catalyst prepared by ultrasonic spray precipitation technique in the synthesis of methanol via CO_2 hydrogenation. *Fuel Process. Technol.* **2018**, *169*, 191–198. [CrossRef]
59. Zhang, Y.; Zhong, L.; Wang, H.; Gao, P.; Li, X.; Xiao, S.; Ding, G.; Wei, W.; Sun, Y. Catalytic performance of spray-dried Cu/ZnO/Al_2O_3/ZrO_2 catalysts for slurry methanol synthesis from CO_2 hydrogenation. *J. CO2 Util.* **2016**, *15*, 72–82. [CrossRef]